NANO LETTERS
Letter
Cite This: Nano Lett. 2018, 18, 6427−6433
pubs.acs.org/NanoLett

Dynamics of Nanoscale Dendrite Formation in Solution Growth Revealed Through in Situ Liquid Cell Electron Microscopy

Matthew R. Hauwiller,[†,‡,⬡] Xiaowei Zhang,[†,§,⬡] Wen-I Liang,[†,∥,⬡] Chung-Hua Chiu,[†,∥,⬡] Qian Zhang,[⊥] Wenjing Zheng,[†,#] Colin Ophus,[▽] Emory M. Chan,[▽] Cory Czarnik,[○] Ming Pan,[○] Frances M. Ross,[▲] Wen-Wei Wu,[∥] Yin-Hao Chu,[∥] Mark Asta,[†,◆] Peter W. Voorhees,[⊥] A. Paul Alivisatos,[†,‡,◆,¶] and Haimei Zheng*[,†,◆]

[†]Materials Sciences Division, Lawrence Berkeley National Laboratory, Berkeley, California 94720, United States
[‡]Department of Chemistry, University of California, Berkeley, California 94720, United States
[§]National Laboratory of Solid State Microstructures, School of Electronic Science and Engineering, and Collaborative Innovation Centre of Advanced Microstructures, Nanjing University, Nanjing, 210093, China
[∥]Department of Materials Science and Engineering, National Chiao Tung University, Hsinchu, 30010, Taiwan
[⊥]Department of Materials Science and Engineering, Northwestern University, 2220 Campus Drive, Evanston, Illinois 60208, United States
[#]Institute of New-Energy Materials, School of Materials Science and Engineering, Tianjin University, Tianjin 300350, China
[▽]The Molecular Foundry, Lawrence Berkeley National Laboratory, Berkeley, California 94720, United States
[○]Gatan Incorporated, Pleasanton, California 94588, United States
[▲]IBM T. J. Watson Research Center, Yorktown Heights, New York 10598, United States
[◆]Department of Materials Science and Engineering, University of California, Berkeley, California 94720, United States
[¶]Kavli Energy NanoScience Institute, University of California—Berkeley and Lawrence Berkeley National Laboratory, Berkeley, California 94720, United States

Supporting Information

ABSTRACT: Formation mechanisms of dendrite structures have been extensively explored theoretically, and many theoretical predictions have been validated for micro- or macroscale dendrites. However, it is challenging to determine whether classical dendrite growth theories are applicable at the nanoscale due to the lack of detailed information on the nanodendrite growth dynamics. Here, we study iron oxide nanodendrite formation using liquid cell transmission electron microscopy (TEM). We observe "seaweed"-like iron oxide nanodendrites growing predominantly in two dimensions on the membrane of a liquid cell. By tracking the trajectories of their morphology development with high spatial and temporal resolution, it is possible to explore the relationship between the tip curvature and growth rate, tip splitting mechanisms, and the effects of precursor diffusion and depletion on the morphology evolution. We show that the growth of iron oxide nanodendrites is remarkably consistent with the existing theoretical predictions on dendritic morphology evolution during growth, despite occurring at the nanoscale.

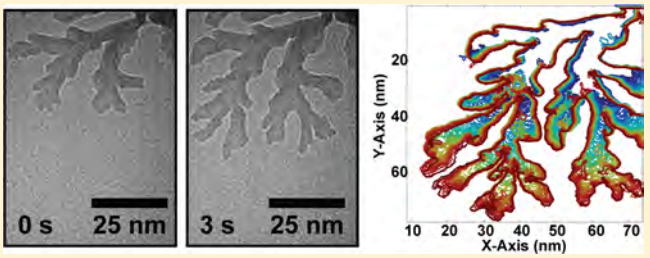

KEYWORDS: *Liquid cell TEM, in situ TEM, nanodendrite, dendrite theories, "seaweed" growth, tip splitting*

Materials with dendritic morphology are found widely in nature (such as snowflakes, coral reefs, seaweed, and trees), and artificial dendritic structures across a wide range of length scales can be synthesized through solidification of metals and alloys, biomineralization, polymerization, and colloidal chemical synthesis.[1] There has been significant recent interest in nanoscale dendrites due to their potential applications in catalysis,[2−8] sensing,[9,10] biological imaging,[11,12] and cancer research.[13,14] An understanding of the pattern formation mechanisms may enable fine control of the fractal morphology and enhance their properties. Extensive studies can be found on micro- and macroscale dendritic structures, and their growth mechanisms have been explored using theoretical approaches with high fidelity. For example, the theory of Mullins and Sekerka[15,16] establishes that instabilities

Received: July 10, 2018
Revised: September 21, 2018
Published: September 26, 2018

DOI: 10.1021/acs.nanolett.8b02819
Nano Lett. 2018, 18, 6427−6433

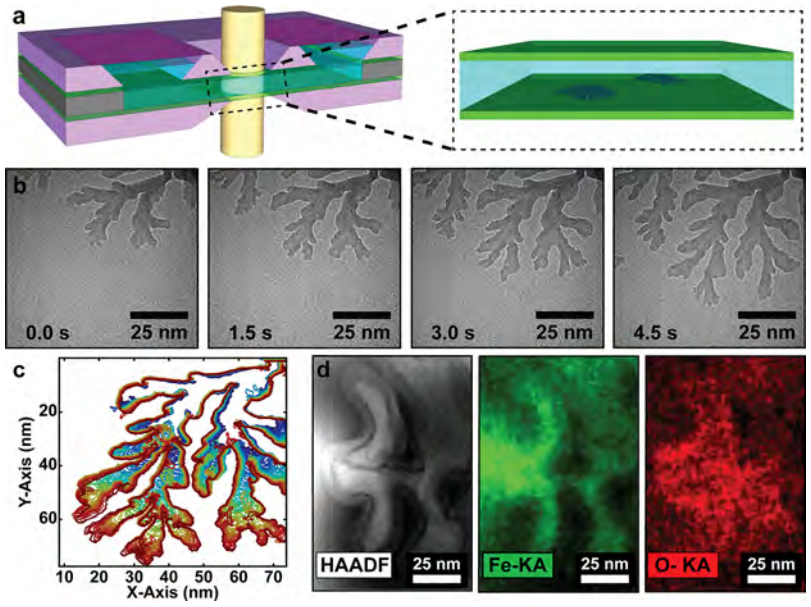

Figure 1. Growth of iron oxide dendritic nanostructures, "seaweed", observed using liquid cell TEM. (a) Schematic of liquid cell setup with the iron oxide "seaweed" nanostructures growing on the silicon nitride membrane. (b) Sequential images from an in situ TEM movie showing the growth of iron oxide "seaweed" nanostructures. (c) Outlines of the iron oxide nanostructures from each frame and overlaid on each other. Color shows time sequence with blue as the initial time and red as the later time. (d) HAADF STEM image and the corresponding EDS elemental maps of the iron oxide "seaweed" nanostructure after drying the sample.

along the interface of growing materials initiate dendritic growth due to competition between mass transport at solid–liquid interfaces and surface tension.[17] This theory can be used to describe many systems where the growth medium is initially homogeneous, and the evolution of local fluctuations leads to formation of dendrites. Microscopic solvability theory of the steady-state dendrite growth[18−21] reveals that the anisotropy of growing crystals determines the growth rate and tip radius of dendrites, even though their growth directions are not limited to a discrete set of crystallographic directions.[22] If there is no crystallographic anisotropy in the growth kinetics or interfacial energy, the structures exhibit tip splitting resulting in "seaweed"-like fractal patterns.[23] The dendrite growth and tip splitting with respect to instabilities[15−17,24] predicted by theory have been largely validated for micro- and macroscale structures using phase-field simulations,[25−30] molecular dynamics (MD),[31−34] and other computational methods.[35,36] However, whether these theoretical predictions are applicable to nanodendrite growth is unknown. Some unique phenomena present at the nanoscale may be neglected by classical dendrite growth theories. For example, large stress induced by surface or interfaces has been found in the nanoparticle growth.[37] Testing the applicability of classical dendrite theories at the nanoscale is challenging due to the difficulties in tracing the fine details of nanodendrite development.

Recent advances in liquid cell transmission electron microscopy (TEM) provide the opportunity to test the dendrite growth theories in the nanoregime. Liquid cell TEM has been used to study various dynamic phenomena in liquids and at solid–liquid interfaces including colloidal nanocrystal growth,[38−43] etching,[44−46] electrochemical deposition,[47−49] and the growth of branched nanostructures such as Pd,[47] Pb,[50] and Au.[51−53] Although the growth of nanoscale dendrites has been observed previously,[47,50−53] tracking the complex fractal nanostructure formation in liquids with high spatial and temporal resolution allowing for testing of the dendrite theories has not been achieved so far. Here, we study iron oxide nanodendrite growth using liquid cell TEM with fine control of the growth conditions, advanced data collection, and image analysis. Through detailed analyses of the nanodendrite growth trajectories within the context of dendrite theories, we elucidate the growth mechanisms of nanodendrites and verify the applicability of these theories at the nanoscale.

We select iron oxide as a model system for dendrite formation due to its numerous applications in catalysis[54,55] and biological imaging.[56] Real time imaging of the growth of iron oxide nanodendrites formation is achieved with high spatial (1.5 Å information limit) and temporal (400 frames per second) resolution (see Methods in the Supporting Information). Tracking nanodendrite growth and tip splitting trajectories reveal the relationship between tip curvature and growth rate, tip splitting mechanisms, and the effects of precursor diffusion/depletion on the morphology evolution. The growth of iron oxide nanodendrites in a liquid cell is found to be remarkably consistent with the theoretical predictions on the "seaweed" growth and presence of tip splitting with respect to instabilities.

Using liquid cell TEM, we image the formation of iron oxide nanodendrite structures in real time. These structures grow from a solution of iron nitrate dissolved in a mixture of oleylamine, oleic acid, and benzyl ether. Initially, a burst of nanoclusters is observed under electron beam illumination, which is similar to the previously reported nanoparticle formation through oleylamine-promoted electron beam reduction.[41−43] Here, the concentration of metal (iron) ions in the growth solution is about 10 times higher than those for regular colloidal nanoparticle growth in a liquid cell.[57,58] We find the nanoclusters grow to 4−6 nm in diameter and they subsequently develop into nanodendrites due to oversaturation induced instabilities. The growth of nanodendrites is mainly two-dimensional on the silicon nitride membrane window with

DOI: 10.1021/acs.nanolett.8b02819
Nano Lett. 2018, 18, 6427−6433

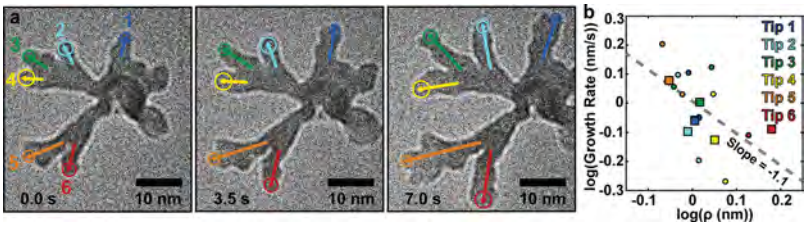

Figure 2. Growth rate of the "seaweed" branches correlated to the curvature of their tips. (a) Sequential images showing the growing "seaweed". The distance from a reference point to the tip and the local curvature of tip were measured. Note that each tip had no competition for precursor and no tip splitting occurred. (b) Logarithm plot of the growth rate vs radius of curvature (ρ) of the tip. Colors correspond to tips in part a, and circles are for linear regions of the growth trajectory while squares are averages over all the frames. The slope of the linear fit is −1.1.

the approximately similar thickness of 4−6 nm as the nanoclusters (without obvious changes in the image contrast). Growth in the vertical direction has also been identified for some branches (Figure S5 and Movie S1), however, the vertical growth is limited likely due to the precursor depletion/diffusion associated with the thin liquid inside the liquid cell. The liquid thickness varies in the liquid cell during imaging (thinner than the original 100 nm liquid film during liquid loading). In order to achieve high resolution imaging thinner liquid (e.g., 20−50 nm) is preferred, which can be obtained under strong electron beam illumination (see details on liquid loading, imaging and electron dose rate in Methods). We describe the nanodendrite patterns as "seaweed" nanostructures,[23,59] of which each dendritic branch does not have well-defined growth direction. We also find the presence of nanobubbles in the liquid influences the fine details of the "seaweed" morphology development (Figure S6); thus bubbles are avoided in this study.

The fractal morphology development of the "seaweed" nanostructure is shown in Figure 1b (also see Movie S2). We trace the contour of the nanostructure during growth using a MATLAB program developed by us (see details in Supporting Information). Figure 1c shows the growth trajectories, where the color gradient from blue to red represents the time lapse from the beginning to the end. The fractal dimensions (D) are calculated to be in the range from 1.8 to 1.9 (see the fractal dimension calculation in Supporting Information), which is close to the value of 1.71 predicted by simulation of diffusion-limited aggregation (DLA) for two-dimensional growth.[60] The observed fine details of the "seaweed" nanostructures are also consistent with the predictions of fractal seaweed and compact seaweed structures, as shown in the Brener's morphology diagram.[23]

The pattern formation from a homogeneous liquid solution generally results from the competition between two dominant factors. One is the capillarity or interfacial energy, which tends to stabilize the solid−liquid interface morphology. For instance, the isotropic surface energy leads to the formation of a sphere. The other factor is diffusion, which drives an interfacial instability.[61] Since surface energy governs during growth at the nanoscale, one would expect to achieve the morphology determined by surface energy minimization (i.e., Wulff shape), and thus nanoparticles. However, the "seaweed" or dendrite morphology can be obtained when supersaturation is sufficiently large. Specifically, the classical Mullins and Sekerka analysis of a growing spherical particle indicates that the particle is unstable when its radius is seven times the critical radius for nucleation.[16] We observe morphological instabilities of domains on the order of 5 nm, so the critical radius for nucleation is very small, likely a result of a large supersaturation (see Supporting Information).

After the in situ imaging, the liquid cell sample is dried at room temperature and opened to perform elemental analysis. Energy dispersive X-ray spectroscopy (EDS) elemental maps reveal that the nanodendrite arms are composed of iron and oxygen (Figure 1d). The more ambiguous distribution of oxygen is due to oxygen being present in the solvent mixture. It is also noted that the as-grown "seaweed" nanostructure is amorphous and it transforms into crystalline Fe_2O_3 and Fe_3O_4 under the prolonged electron beam illumination (Figure S7). This suggests that the amorphous structure results from the fast growth kinetics.[62] Choosing an amorphous material in this study eliminates the crystalline anisotropy when relating to dendrite growth theories.

In order to study the correlation between the tip curvature and growth rate, we first determine the factors that control the growth of a single tip in an environment unencumbered by other dendritic branches. The dendrite shown in Figure 2a exhibits six distinctive tips growing outward from the center with enough separation between tips such that influence from the neighboring branches is minimized. In addition, none of the tips split in the duration of time being analyzed. We measure the growth rate of a tip with the assumption that the tip grows approximately unidimensionally, which is an accepted method for measuring dendritic growth.[17,63] The distance between each tip and a point normal to the growth direction of the tip is measured for each frame of the image sequences in the movie. The logarithm of growth rate of each dendritic tip as a function of the logarithm of the radius of curvature (ρ) is plotted, as shown in Figure 2b, where radius of curvature is the radius of a circle fit to the tip. We find that sharper tip curvature is correlated with faster growth.

The observed relationship between the tip curvature and growth rate is consistent with a diffusion controlled dendritic growth model.[17,63,64] As expected, the tips with higher curvature exhibit faster growth rates since the larger the curvature, the higher the concentration gradient at the tip.[17] A few factors have been considered for the tip growth of these "seaweed" nanostructures. First, diffusion in a thin liquid layer inside a liquid cell is several orders of magnitude slower than those in bulk liquids.[65] Second, the tip curvature of these nanoscale dendrites is extremely high compared to bulk dendrites. Finally, the oversaturation of the precursor solution plays an important role. Although there is an interplay between these different factors during tip growth, the observed trend of tip growth as a function of tip curvature suggests that the energy barrier for the monomer addition is insignificant compared to the barrier for monomer diffusion into the tip

DOI: 10.1021/acs.nanolett.8b02819
Nano Lett. 2018, 18, 6427−6433

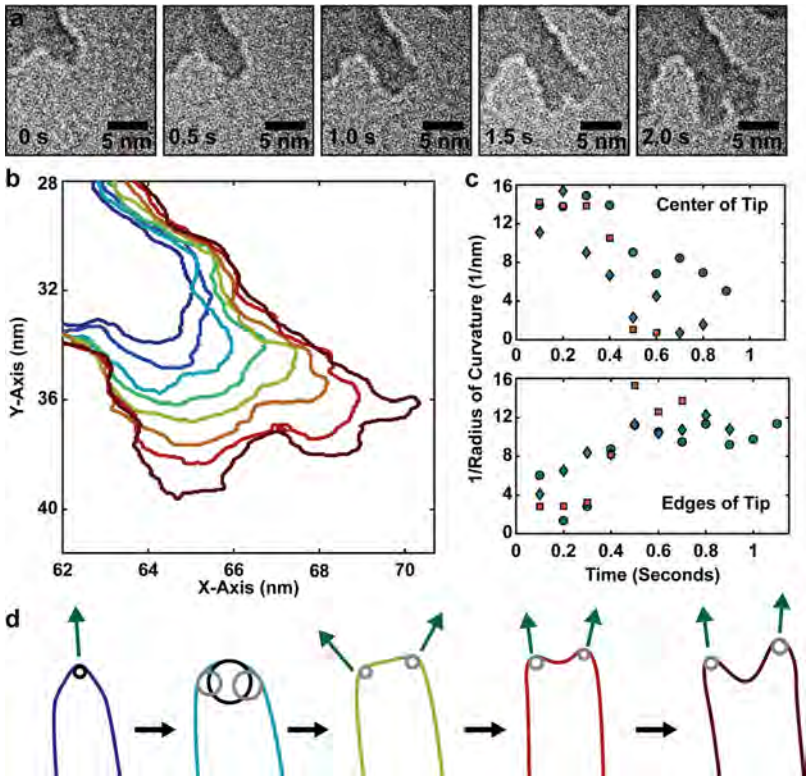

Figure 3. Tip splitting process. (a) Sequential images showing a tip splits into two equivalent new tips growing into two branches. (b) Outlines of the splitting tip in part a. The original single tip (blue) widens and grows on the corners of the flattened top (red). (c) Measured curvature at the center and edges of the tip during the splitting process. Initially, the tip has the greatest curvature at the center and then it becomes flat with the edges of the tip developing high curvature. (d) Schematic showing the tip splitting process.

front. The relationship between the tip curvature and growth rate is linear, as predicted by Ivanstov in 1947[66] (Figure 2b).

The growing tips are morphologically unstable. Branching of the growing "seaweed" structure, or tip splitting, controls the fractal morphology. A representative example of a splitting tip is shown in Figure 3a, in which a single growing tip bifurcates into two new tips and each continues to grow. The outlines of the tip show the splitting process, where the color gradient from blue to red represents the time lapse (Figure 3b). It is clear that the initially sharp tip undergoes flattening and widening before splitting into two distinct tips. The curvature changes during the tip splitting process are measured. As the initial tip widens, the curvature at the center of the tip decreases and the curvature at the sides increases (Figure 3c). We consider the initial widening of a growing tip results from fluctuations during growth. Since the sharper curvature grows faster, the faster growth at the edges of the tip leads to two new tips (see the schematic in Figure 3d).

This observed tip splitting process can be explained by the established analytical models describing dendrite tip splitting with respect to instabilities.[15−17,24] According to these models, a dendrite tip splits when the tip radius becomes larger than the shortest wavelength of morphological instability.[15] The tip widening and splitting have been demonstrated experimentally and computationally on the micrometer scale.[59] Dendritic growth on the micrometer scale leads to asymmetric growth associated with the crystalline anisotropy.[67] In contrast, although the nanoscale dendrite structures exhibit no crystalline anisotropy (it is amorphous), it also demonstrates the asymmetric growth during which one of the two new tips grows faster and soon becomes dominant. Therefore, the tip-splitting and tip growth behavior we have observed here shows that the established models for tip splitting are applicable at the nanoscale.

Since the growth is diffusion limited, the competition for precursor may strongly influence the "seaweed" morphology. For example, Figure 4a shows a time series of the development of four tips. As the growth progresses, two tips grow and split while the other two tips stop growing and remain as a single tip. The discontinuation of tip growth is independent of the tip curvature. We hypothesize that the growing tips compete for precursor, thus a growing tip impacts the growth of a neighboring tip in close proximity.

To test the above hypothesis, we examine three tips with different configurations of neighbors during the "seaweed" development. As highlighted in Figure 4b, they are marked as the blue, green, and red dots on the growing "seaweed" structure. Along the growth trajectories of each tip, the growth rate varies and the surrounding dendrite density also changes. The dendrite density around a tip is measured by the area ratio occupied by the dendritic branches within the disc of a given radius around the tip. By varying the disc radius, different values of dendrite density (average solid density within the disc) can be achieved. Therefore, at each point on the growth trajectory the tip has a growth rate, which is correlated to different values of the average solid density depending on the calculated disc sizes. We plot the growth rate of the tip as a function of the average solid density and disc size (the distance to the tip within 0−30 nm) during the "seaweed" development (Figure 4c). The growth rate variations are reflected by the different color of the plot.

DOI: 10.1021/acs.nanolett.8b02819
Nano Lett. 2018, 18, 6427−6433

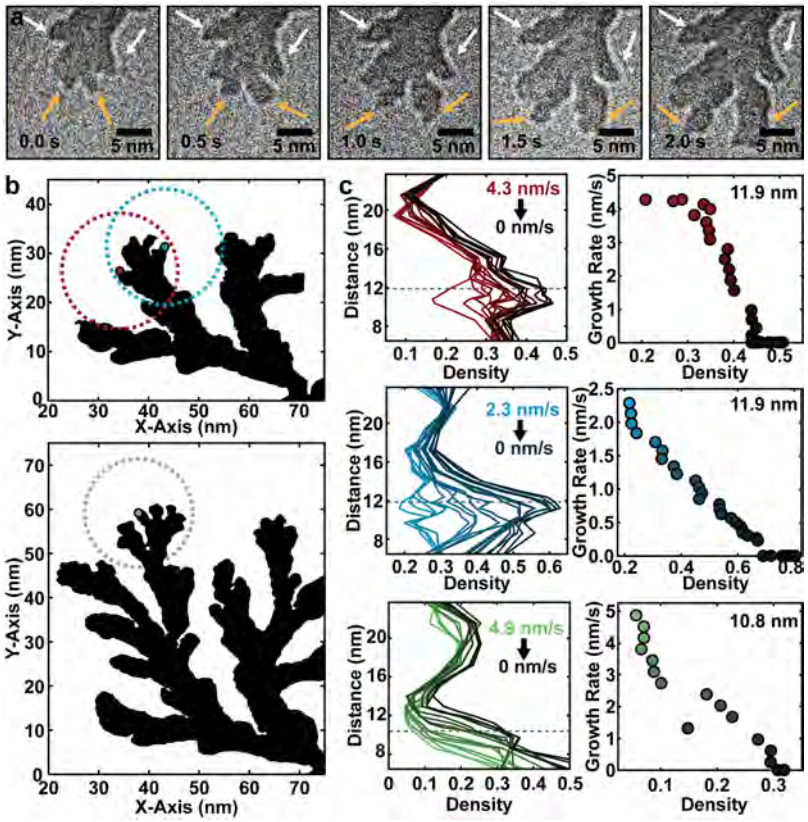

Figure 4. Effect of neighboring branches competing for precursor on growth rate of tips. (a) Sequential images of growing "seaweed" with four tips. Initially, the tips are approximately equivalent in all respects except local density of iron oxide structures. After two seconds, two tips have completely stopped growing (highlighted in white arrows) while the other two tips (highlighted in yellow arrows) have significant growth and even undergone further tip splitting events. (b) The "seaweed" nanostructure at different stages of growth with three tips highlighted in different neighboring environments. (c) Comparing tip growth rate under different "seaweed" density at different distances from the tip. Densities at small and large distances from the tip show less correlation to the growth rate of the tip. However, the density at an average intermediate distance of about 10−12 nm has a strong dependence on the growth rate, which we term the precursor diffusion zone. The growth rates compared with densities at their distance of strongest dependence is shown for each tip. The radius of the rings in part b are the same distances.

From Figure 4c, the correlation between the growth rate and average solid density at a certain disc size during the "seaweed" growth can be obtained. We find a similar trend for most calculated disc sizes that as the average solid density increases the growth rate of the tip decreases and the tip stops growing when the average solid density increases significantly. At the critical disc distance (disc radius r_0 = 10−12 nm), the strongest correlation between the growth rate of the tip and the average solid density is achieved such that the changes of the average solid density induce the largest variations of the growth rate. (also see Figure S8) Above or below the critical distance (r_0), correlation between the average solid density and growth rate is lower although the trend (an increase of the average solid density results in lower growth rate) maintains for most disc sizes. These results suggest that the critical distance corresponds to the precursor diffusion zone around the tip. Within the diffusion zone, all growing dendrites compete for precursor. Therefore, an increase of the dendrite density reduces the chance of precursor reaching the tip thus slowing down the tip growth. The growth rate variations can be more drastic when it is close to the critical distance since larger variations of the average solid density are achieved. Dendrites beyond the diffusion zone has little impact on the growth rate of the tip, thus the correlation between the growth rate and the average solid density decreases when the disc radius is larger than the critical radius. It is noted that in the above analyses the average solid density may deviate from the actual growing dendritic branches competing for precursor, however, the growing front of the "seaweed" has similar characteristics for different tips and thus the analysis still stands.

During the two-dimensional growth of "seaweed" nanostructures, the precursor very close to the "seaweed" is depleted and little replenishment of the precursor from the bulk solution occurs. This is evident because, as the structure grows outward, only the tips furthest from the branching point grow. This is reasonable that the growing tips deplete their local environment of precursor, causing the further growth of the tip to occur only by reaching out in the bulk solution where the precursor can be replenished more rapidly and maintained at higher concentrations.

In summary, the tips with crowded neighbors, i.e., those that are not at the growing front, slow down or completely stop growing as the local precursor is depleted. Within the environment with the presence of precursor, a tip may split and the newly formed tips now compete for precursor. The tip with a sharper curvature grows faster and may become the dominant growing tip, as discussed in the previous section of this paper. Therefore, the combination of precursor depletion/diffusion, curvature dependent growth rate, and tip splitting controls the "seaweed" fractal morphology development. In the growth regime where different tips compete for precursor, the anisotropy of the tip growth is determined by both the growth

DOI: 10.1021/acs.nanolett.8b02819
Nano Lett. 2018, 18, 6427−6433

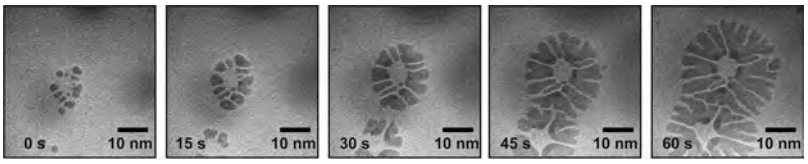

Figure 5. Sequential images show the formation of "spherulite" nanostructure from multiple seeds with close distance. The branches are densely packed with significantly fewer tip splitting events during growth.

rate and the tip radius, which is consistent with the theoretical predictions based on tip splitting with respect to instabilities.[15−17,24]

The effects of neighboring structures on the morphology development of nanodendrites due to different branches competing for precursor are also reflected in the growth of "spherulite"[68] nanostructure. We show the growth of iron oxide nanostructures when multiple seeds are in close distance. Sequential images display multiple seeds developing into "spherulite" nanostructure (Figure 5; also see Movie S5). Each seed growing into one or a few branches with significantly fewer tip splitting events, reminiscent of the structures seen during directional solidification where interactions between neighboring grains are very strong. In this case, branches in the "spherulite" structure are long and densely packed, which implies neighboring branches competing for precursor akin to the neighboring effects during the growth of "seaweed" structure.

In summary, we have been able to trace the fractal morphology development of iron oxide nanodendrites ("seaweed" nanostructures) using liquid cell TEM with high spatial and temporal resolution, which allows the direct comparison of the morphology evolution predicted by the classical theories and the experiments. The growth of the nanodendrites and tip splitting are determined by the growth rate and tip curvature, which is consistent with the dendrite theories on tip splitting with respect to instabilities. We have also found that the neighboring dendrites at close distances influence tip growth, and neighboring dendrites within a critical distance of 10−12 nm, which corresponds to a precursor diffusion zone, have the strongest effect on the tip growth. When multiple branches grown from different seeds grow side-by-side, each growing tip has significantly fewer tip splitting events and they develop into a "spherulite" nanostructure. This work opens many opportunities to explore the development of various nanostructures with fractal morphology in the context of classical dendrite theories. Validation of the dendrite growth theories at the nanoscale shed light on rational design and synthesis of nanostructured materials with complex fractal morphologies.

■ ASSOCIATED CONTENT

Supporting Information

The Supporting Information is available free of charge on the ACS Publications website at DOI: 10.1021/acs.nanolett.8b02819.

Experimental and image analysis methods, additional figures, and details of the movies of iron oxide "seaweed" structures (PDF)

Movie S1, growth of iron oxide nanodendrite "seaweed" nanostructure (AVI)

Movie S2, growth of unencumbered iron oxide "seaweed" nanostructure (AVI)

Movie S3, growth of another unencumbered iron oxide "seaweed" nanostructure (AVI)

Movie S4, growth of iron oxide "seaweed" nanostructure (AVI)

Movie S5, growth of iron oxide nanodendrite "spherulite" nanostructure (AVI)

■ AUTHOR INFORMATION

Corresponding Author

*(H.Z.) E-mail: hmzheng@lbl.gov.

ORCID

Matthew R. Hauwiller: 0000-0002-5448-6937
Wen-Wei Wu: 0000-0002-8388-8417
Yin-Hao Chu: 0000-0002-3435-9084
A. Paul Alivisatos: 0000-0001-6895-9048
Haimei Zheng: 0000-0003-3813-4170

Author Contributions

⬡These authors contributed equally to this work

Notes

The authors declare no competing financial interest.

■ ACKNOWLEDGMENTS

This work was funded by the U.S. Department of Energy, Office of Science, Office of Basic Energy Sciences, Materials Sciences and Engineering Division, under Contract No. DE-AC02-05-CH11231 within the insitu TEM program (KC22ZH). Work at the Molecular Foundry was supported by the Office of Science, Office of Basic Energy Sciences, of the U.S. Department of Energy, under Contract No. DE-AC02-05CH11231. We acknowledge Gatan Inc. for the advanced K2 IS camera. M.R.H. acknowledges the support of a KAUST CRG grant at UC Berkeley. C.-H.C. was funded by Ministry of Science and Technology (MOST) in Taiwan (Grant 103-2917-I-009-185). W.-I.L. was partially funded by MOST in Taiwan (NSC 102-2119-I-009-502). X.Z. acknowledges the support of the National Basic Research Program of China (2013CB632101) and China Scholarship Council under Grant No. 201406190080. The authors declare no competing financial interests.

■ REFERENCES

(1) Meakin, P. *Fractals, Scaling and Growth Far from Equilibrium*; Cambridge University Press: Cambridge, U.K., 1998.
(2) Pan, M.; Xing, S.; Sun, T.; Zhou, W.; Sindoro, M.; Teo, H. H.; Yan, Q.; Chen, H. *Chem. Commun.* **2010**, *46*, 7112.
(3) Li, X.-R.; Li, X.-L.; Xu, M.-C.; Xu, J.-J.; Chen, H.-Y. *J. Mater. Chem. A* **2014**, *2*, 1697−1703.
(4) Zhang, J.; Li, K.; Zhang, B. *Chem. Commun.* **2015**, *51*, 12012−12015.
(5) Jiang, B.; Li, C.; Malgras, V.; Bando, Y.; Yamauchi, Y. *Chem. Commun.* **2016**, *52*, 1186−1189.
(6) Watt, J.; Cheong, S.; Toney, M. F.; Ingham, B.; Cookson, J.; Bishop, P. T.; Tilley, R. D. *ACS Nano* **2010**, *4*, 396−402.

DOI: 10.1021/acs.nanolett.8b02819
Nano Lett. 2018, 18, 6427−6433

(7) Lim, B.; Jiang, M.; Camargo, P. H. C.; Cho, E. C.; Tao, J.; Lu, X.; Zhu, Y.; Xia, Y. *Science* **2009**, *324*, 1302−1305.
(8) Lim, B.; Jiang, M.; Yu, T.; Camargo, P. H. C.; Xia, Y. *Nano Res.* **2010**, *3*, 69−80.
(9) Wen, X.; Xie, Y.-T.; Mak, W. C.; Cheung, K. Y.; Li, X.-Y.; Renneberg, R.; Yang, S. *Langmuir* **2006**, *22*, 4836−4842.
(10) Qiu, R.; Zhang, X. L.; Qiao, R.; Li, Y.; Kim, Y. Il; Kang, Y. S. *Chem. Mater.* **2007**, *19*, 4174−4180.
(11) Jia, W.; Li, J.; Jiang, L. *ACS Appl. Mater. Interfaces* **2013**, *5*, 6886−6892.
(12) Liu, X.; Zhang, X.; Zhu, M.; Lin, G.; Liu, J.; Zhou, Z.; Tian, X.; Pan, Y. *ACS Appl. Mater. Interfaces* **2017**, *9*, 279−285.
(13) Qiu, P.; Yang, M.; Qu, X.; Huai, Y.; Zhu, Y.; Mao, C. *Biomaterials* **2016**, *104*, 138−144.
(14) Ma, N.; Wu, F.-G.; Zhang, X.; Jiang, Y.-W.; Jia, H.-R.; Wang, H.-Y.; Li, Y.-H.; Liu, P.; Gu, N.; Chen, Z. *ACS Appl. Mater. Interfaces* **2017**, *9*, 13037−13048.
(15) Mullins, W. W.; Sekerka, R. F. *J. Appl. Phys.* **1964**, *35*, 444−451.
(16) Mullins, W. W.; Sekerka, R. F. *J. Appl. Phys.* **1963**, *34*, 323−329.
(17) Langer, J. S. *Rev. Mod. Phys.* **1980**, *52*, 1−28.
(18) Langer, J. S. *Chance and Matter* **1987**, *395*, 629−711.
(19) Barbieri, A.; Langer, J. S. *Phys. Rev. A: At., Mol., Opt. Phys.* **1989**, *39*, 5314−5325.
(20) Kessler, D. A.; Koplik, J.; Levine, H. *Adv. Phys.* **1988**, *37*, 255−339.
(21) Ben Amar, M.; Brener, E. *Phys. Rev. Lett.* **1993**, *71*, 589−592.
(22) Haxhimali, T.; Karma, A.; Gonzales, F.; Rappaz, M. *Nat. Mater.* **2006**, *5*, 660−664.
(23) Brener, E.; Müller-Krumbhaar, H.; Temkin, D. *Phys. Rev. E: Stat. Phys., Plasmas, Fluids, Relat. Interdiscip. Top.* **1996**, *54*, 2714−2722.
(24) Turing, A. M. *Philos. Trans. R. Soc., B* **1952**, *237*, 37−72.
(25) Karma, A.; Rappel, W.-J. *Phys. Rev. Lett.* **1996**, *77*, 4050−4053.
(26) Karma, A.; Rappel, W.-J. *Phys. Rev. E: Stat. Phys., Plasmas, Fluids, Relat. Interdiscip. Top.* **1998**, *57*, 4323−4349.
(27) Karma, A. Phase Field Methods. In *Encyclopedia of Materials: Science and Technology*; Elsevier, 2001; pp 6873−6886.
(28) Plapp, M.; Karma, A. *Phys. Rev. Lett.* **2000**, *84*, 1740−1743.
(29) Plapp, M.; Karma, A. *J. Comput. Phys.* **2000**, *165*, 592−619.
(30) Provatas, N.; Goldenfeld, N.; Dantzig, J. *Phys. Rev. Lett.* **1998**, *80*, 3308−3311.
(31) Asta, M.; Hoyt, J. J.; Karma, A. *Phys. Rev. B: Condens. Matter Mater. Phys.* **2002**, *66*, 100101.
(32) Sun, D. Y.; Asta, M.; Hoyt, J. J. *Phys. Rev. B: Condens. Matter Mater. Phys.* **2004**, *69*, 024108.
(33) Morris, J. R. *Phys. Rev. B: Condens. Matter Mater. Phys.* **2002**, *66*, 144104.
(34) Sun, D. Y.; Mendelev, M. I.; Becker, C. A.; Kudin, K.; Haxhimali, T.; Asta, M.; Hoyt, J. J.; Karma, A.; Srolovitz, D. J. *Phys. Rev. B: Condens. Matter Mater. Phys.* **2006**, *73*, 024116.
(35) Liu, S.; Napolitano, R. E.; Trivedi, R. *Acta Mater.* **2001**, *49*, 4271−4276.
(36) Napolitano, R. E.; Liu, S. *Phys. Rev. B: Condens. Matter Mater. Phys.* **2004**, *70*, 214103.
(37) Shchukin, V. A.; Bimberg, D. *Rev. Mod. Phys.* **1999**, *71*, 1125−1171.
(38) Li, D.; Nielsen, M. H.; Lee, J. R. I.; Frandsen, C.; Banfield, J. F.; De Yoreo, J. J. *Science* **2012**, *336*, 1014−1018.
(39) Yuk, J. M.; Park, J.; Ercius, P.; Kim, K.; Hellebusch, D. J.; Crommie, M. F.; Lee, J. Y.; Zettl, A.; Alivisatos, A. P. *Science* **2012**, *336*, 61−64.
(40) *Liquid Cell Electron Microscopy*; Ross, F. M., Ed.; Cambridge University Press: Cambridge, U.K., 2016.
(41) Zheng, H.; Smith, R. K.; Jun, Y.; Kisielowski, C.; Dahmen, U.; Alivisatos, A. P. *Science* **2009**, *324*, 1309−1312.
(42) Liao, H.-G.; Cui, L.; Whitelam, S.; Zheng, H. *Science* **2012**, *336*, 1011−1014.
(43) Liao, H.-G.; Zherebetskyy, D.; Xin, H.; Czarnik, C.; Ercius, P.; Elmlund, H.; Pan, M.; Wang, L.-W.; Zheng, H. *Science* **2014**, *345*, 916−919.
(44) Ye, X.; Jones, M. R.; Frechette, L. B.; Chen, Q.; Powers, A. S.; Ercius, P.; Dunn, G.; Rotskoff, G. M.; Nguyen, S. C.; Adiga, V. P.; et al. *Science* **2016**, *354*, 874−877.
(45) Wu, J.; Gao, W.; Yang, H.; Zuo, J.-M. *ACS Nano* **2017**, *11*, 1696−1703.
(46) Hauwiller, M. R.; Ondry, J. C.; Alivisatos, A. P. *J. Visualized Exp.* **2018**, 1−9.
(47) Zhu, G.; Jiang, Y.; Lin, F.; Zhang, H.; Jin, C.; Yuan, J.; Yang, D.; Zhang, Z. *Chem. Commun.* **2014**, *50*, 9447.
(48) Zeng, Z.; Liang, W.-I.; Liao, H.-G.; Xin, H. L.; Chu, Y.-H.; Zheng, H. *Nano Lett.* **2014**, *14*, 1745−1750.
(49) Zeng, Z.; Zhang, X.; Bustillo, K.; Niu, K.; Gammer, C.; Xu, J.; Zheng, H. *Nano Lett.* **2015**, *15*, 5214−5220.
(50) White, E. R.; Singer, S. B.; Augustyn, V.; Hubbard, W. A.; Mecklenburg, M.; Dunn, B.; Regan, B. C. *ACS Nano* **2012**, *6*, 6308−6317.
(51) Kraus, T.; De Jonge, N. *Langmuir* **2013**, *29*, 8427−8432.
(52) Ahmad, N.; Le Bouar, Y.; Ricolleau, C.; Alloyeau, D. *Adv. Struct. Chem. Imaging* **2017**, *2*, 9.
(53) Zhang, Y.; Keller, D.; Rossell, M. D.; Erni, R. *Chem. Mater.* **2017**, *29*, 10518−10525.
(54) Zeng, S.; Tang, K.; Li, T.; Liang, Z.; Wang, D.; Wang, Y.; Qi, Y.; Zhou, W. *J. Phys. Chem. C* **2008**, *112*, 4836−4843.
(55) Zhong, L. S.; Hu, J. S.; Liang, H. P.; Cao, A. M.; Song, W. G.; Wan, L. J. *Adv. Mater.* **2006**, *18*, 2426−2431.
(56) Laurent, S.; Forge, D.; Port, M.; Roch, A.; Robic, C.; Vander Elst, L.; Muller, R. N. *Chem. Rev.* **2010**, *110*, 2574−2574.
(57) Liang, W. I.; Zhang, X.; Bustillo, K.; Chiu, C. H.; Wu, W. W.; Xu, J.; Chu, Y. H.; Zheng, H. *Chem. Mater.* **2015**, *27*, 8146−8152.
(58) Liang, W.-I.; Zhang, X.; Zan, Y.; Pan, M.; Czarnik, C.; Bustillo, K.; Xu, J.; Chu, Y.-H.; Zheng, H. *J. Am. Chem. Soc.* **2015**, *137*, 14850−14853.
(59) Chen, Y.; Billia, B.; Li, D. Z.; Nguyen-Thi, H.; Xiao, N. M.; Bogno, A. A. *Acta Mater.* **2014**, *66*, 219−231.
(60) Ihle, T.; Müller-Krumbhaar, H. *Phys. Rev. Lett.* **1993**, *70*, 3083−3086.
(61) Müller-Krumbhaar, H.; Zimmer, M.; Ihle, T.; Saito, Y. *Phys. A* **1996**, *224*, 322−337.
(62) Spassov, T.; Köster, U. *J. Alloys Compd.* **1999**, *287*, 243−250.
(63) Doherty, R. D. Dendritic Growth. In *Crystal Growth*; Pergamon Press: Oxford, U.K., 1980; pp 485−520.
(64) Kurz, W.; Fisher, D. J. *Acta Metall.* **1981**, *29*, 11−20.
(65) Zheng, H.; Claridge, S. a.; Minor, a M.; Alivisatos, A. P.; Dahmen, U. *Nano Lett.* **2009**, *9*, 2460−2465.
(66) Ivantsov, G. P. *Dokl. Akad. Nauk. SSSR* **1947**, *58*, 567−569.
(67) Utter, B.; Ragnarsson, R.; Bodenschatz, E. *Phys. Rev. Lett.* **2001**, *86*, 4604−4607.
(68) Keith, H. D. *Kolloid Z. Z. Polym.* **1969**, *231*, 421−438.

DOI: 10.1021/acs.nanolett.8b02819
Nano Lett. 2018, 18, 6427−6433